Revista Boliviana de Química, 2025, Vol. 42, N°2, 155-166
Víctor Hugo Cavero-Olguin et al.
https://doi.org/10.53287/pyii9560fa25m

Original article [1]

Molecular docking analysis of 1,8-cineole with SARS-CoV-2 main protease M^{pro} and macrodomain MacI: insights into potential weak interactions

Víctor Hugo Cavero-Olguin,[1] Natalie N. Escobar-Flores,[1] José A. Bravo,[1] Patricia Mollinedo,[1] José L. Vila,[1] Javier A. Linares-Pastén[2,*]

[1]Instituto de Investigaciones Químicas IIQ, Universidad Mayor de San Andrés UMSA, Av. Villazón N° 1995, La Paz, Bolivia;
[2]Department of Biotechnology, Faculty of Engineering, Lunds Tekniska Högskola (LTH), Lund University, Lund, Sweden

Keys: *COVID-19, Molecular docking, 1,8-cineole;* **Claves:** *COVID-19, Acoplamiento molecular, 1,8-cineol.*

ABSTRACT

Molecular docking is a computational approach that predicts interactions between ligands and protein targets based on binding energies. In this study, the potential interactions of 1,8-cineole -one of the dominant components of *Eucalyptus globulus* oil- with the main protease (M^{pro}) and macrodomain (MacI) of SARS-CoV-2 were studied by molecular docking. Nine M^{pro} and four ManI structures available in the Protein Data Bank (PDB) were assessed as receptors. The results showed binding affinities ranging from −2.1 to −6.3 kcal/mol, primarily mediated by hydrophobic interactions. The most stable complexes were obtained with MacI (PDB: 5RVR, −6.380 kcal/mol) and M^{pro} (PDB: 5R81, −5.402 kcal/mol). Although the interactions are relatively weak, these results suggest that 1,8-cineole may interact with the SARS-CoV-2 M^{pro} and MacI, and provide a basis for further experimental studies to validate its effect. Since eucalyptus oil vapor is widely used in the Andean region of Bolivia to prevent respiratory ailments, this work offers an initial *in silico* rationale for such traditional practices.

RESUMEN

El acoplamiento molecular es una técnica computacional que permite predecir cómo interactúan ligandos con proteínas, basándose en sus energías de enlace. En esta investigación, se estudió el 1,8-cineol, compuesto principal del aceite esencial de *Eucalyptus globulus*, frente a dos proteínas del SARS-CoV-2: la proteasa principal (Mpro) y el macrodominio (MacI). Se analizaron nueve estructuras de Mpro y cuatro de MacI disponibles en el Protein Data Bank. Las afinidades de enlace obtenidas variaron entre −2,1 y −6,3 kcal/mol, predominando las interacciones hidrofóbicas. Los complejos más estables se observaron con MacI (PDB: 5RVR) y Mpro (PDB: 5R81). Aunque las interacciones fueron moderadas, los resultados sugieren que el 1,8-cineol podría unirse a estas proteínas virales, lo que abre la puerta a estudios experimentales. Dado que el vapor de eucalipto se usa tradicionalmente en la región andina de Bolivia para prevenir afecciones respiratorias, este estudio aporta una primera base científica a dicha práctica.

Revista Boliviana de Química, 2025, 42, 155-166
ISSN 0250-5460, Rev. Bol. Quim. *Paper edition*
ISSN 2078-3949, Rev. boliv. quim. *e-edition*, *May-Nov*
30 noviembre 2025, https://doi.org/10.53287/pyii9560fa25m

https://bolivianchemistryjournaliiq.umsa.bo

[1]Received September 18, 2025, accepted November 10, 2025, published November 30, 2025. *Mail to: javier.linares-pasten@ple.lth.se

INTRODUCTION

Several natural compounds with applications to different health problems and conditions are found in plants used in traditional medicine around the world. One good example is the cyclic ether and monoterpenoid 1,8-cineole, also known as eucalyptol. Produced by different plants belonging to *Myrtaceae*, *Lamiaceae,* and *Zingiberaceae* families, there are more than 900 species in the genus *Eucalyptus* from *Myrtaceae*. *Eucalyptus kochill* subsp. *Borealis* is considered to be the plant with the highest content of 1,8-cineole since it contains about 97.32 % of it in its essential oil [1]. 1,8-cineole is said to be good at some inflammation-related clinical conditions like colitis, asthma, and pancreatitis, as an active compound plays an important role in the treatment of respiratory diseases, cancers, digestive disorders, dysphoria, Alzheimer's disease (AD), cardiovascular illnesses, and others, seemingly decreasing pro-inflammatory cytokine levels [2]. It was reported that it enhanced antioxidant enzyme activities, attenuating oxidative stress and inflammation [3].

Different levels of antibacterial interaction of 1,8-cineole were seen in various studies, ranging from interference with carbohydrate metabolism, interference with the outer membrane protein synthesis at the mRNA level, to enhancing the absorption of amoxicillin in the intestines while prolonging its half-life as well. Other mechanisms include synergistic action with different antibiotics, lowering the affinity for β-lactamase enzyme activity. An interesting synergistic effect has been seen with penicillin G and amoxicillin when 1,8-cineole was used in concentrations below the inhibitory effect [4]. It was shown that it interfered with the synthesis of metabolites implicated in quorum sensing, a fundamental process in the development of biofilms-structures that enhance antibiotic resistance [5]. Similar action of controlling the formation of biofilms was seen in treatments against pathogenic fungi like *Fusarium solani, Candida albicans,* and *Candida glabrata* after *in vitro* treatment with 1,8-cineole [6]. The antimicrobial activity remains to be discovered, and its use could be enhanced by its use with other antimicrobial agents. Up to now, the proper mechanisms by which 1,8-cineole exerts an antimicrobial action are still not well understood [1]. The administration of 1,8-cineole is primarily achieved through pharmaceutical presentations, such as capsules, although its poor water solubility results in low absorption in oral, nasal, and pulmonary administrations. The need for better pharmaceutical presentations to enhance absorption is a scope for research.

Control of airborne pathogen microorganisms is a matter of concern, as the spread of various infectious diseases could worsen in the near future [7]. Studies on the effectiveness of antibiotic use in aerosols have demonstrated its efficacy. Polymer-based synthetic mimics of antimicrobial peptides (SMAMPs) suspensions have shown efficacy against *S. aureus* and *E. coli* suspensions, demonstrating antimicrobial activity and, in some cases, even bactericidal effects [8]. Surrounding conditions affect the suspended particles, as all airborne microbes experienced desiccation; gram-negative bacteria and lipid-containing viruses demonstrated phase changes in their outer phospholipid bilayer membranes owing to concomitant changes in water content and/or temperature [9]. Single virus particles rarely persist in the air, as they tend to rapidly aggregate. Therefore, depending on the size and distribution of the airborne particles, virus-laden particles of aerosols are a complex mixture of various components (salts, proteins, and other organic and inorganic matter, including virus particles). It is essential to realize that the size of the viral particle itself does not rule the airborne particle size [10]. Since the SARS-CoV-2 virus is ca. 100 nm in diameter, its ability to penetrate the human aerial upper vias is a fact; therefore, attempts to control its dispersion while suspended could easily mitigate the risk of disease. Since ultrasonic atomization is an effective method for nebulizing 1,8-cineole to mitigate lung or airway injury [1], its use in controlling airborne SARS-CoV-2 could be promising.

Main protease (M^{pro}), also known as main peptidase, 3CL or $3CL^{pro}$ due to its 3-chymotrypsin-like protease/peptidase action, is essential for the SARS-CoV-2 viral life cycle. M^{pro} is uniquely diversified to have an unconventional Cys catalytic residue. The absence of closely related homologues in humans makes inhibitors unlikely to be toxic; M^{pro} becomes, in this way, an attractive target for the design of antiviral drugs [11,12]. Unlike other chymotrypsin-like enzymes and many Ser (or Cys) hydrolases, it has a catalytic Cys-His dyad instead of a canonical Ser (Cys)-His-Asp (Glu) triad [13]. Moreover, the pocket of M^{pro} is highly conserved among all coronaviruses; therefore, finding a single effective antiviral compound might help prevent more infections by coronaviruses [12]. The crystal structure of M^{pro} in complex with a synthetic peptidomimetic called N3 was reported in 2016 and deposited in the Protein Data Bank (PDB) with the code 6LU7. Docking pose study revealed it to be an irreversible inhibitor that could fit inside the substrate-binding pocket, as shown after docking [12]. While the target-ligand interaction in 6LU7 is of a covalent nature, the natural potent broad-spectrum non-covalent inhibitor X77 was found to form a non-covalent docking with M^{pro}, a complex available in the PDB with the code 6W63. It is considered to be a promising molecular target for the development of compounds that may inhibit this protein [14,15]. Crystal structure 2GX4 (PDB) was seen to be formed

through the interaction of the NOL ligand with a His residue of the side chain through hydrogen bonds. This structure served as a docking study platform for 12 hydroxyxanthone compounds, known for their antiviral activities [16].

On the other hand, recently, the macrodomain of the non-structural protein 3 (NSP3) of SARS-CoV-2 has emerged as an attractive target for antivirals. The macrodomain, also known as MacI, S2-MacroD, or X domain, hydrolyses ADP-ribose moieties from mono-ADP-ribosylated viral proteins, thereby interfering with host antiviral signalling [17]. Additional studies have shown that MacI is fundamental for viral replication. Thus, MacI is an interesting target for 1,8-cineole. The list of structures retrieved from the RCSB PDB considered in this work is shown in Table 1.

Although there have been reports showing strong binding affinities of *Eucalyptus sp*. essential oils against SARS-CoV-2 spike protein and proteases in silico, there are not too many docking reports with 1,8-cineole as a ligand for M^{prot} as target [18], and no studies on 1,8-cineole interaction with MacI. Nonetheless, a study using pseudo-SARS-CoV-2 suggested even a proviral activity of the essential oils [19]. Molecular docking is a widely used computational tool in modern drug discovery, predicting the binding affinity of ligands with the target receptor protein. This work addressed the molecular interactions between 1,8-cineole and SARS-CoV-2 M^{pro} and MacI, suggesting the feasibility of inactivation of the virus.

EXPERIMENTAL

Extraction of *Eucalyptus globulus* oil

Eucalyptus leaves were collected from the town of Quime, La Paz, Bolivia (16°98′25″S 67°24′47″W), at 3000 meters above sea level. A 2500 g sample was size compacted and placed in conventional steam stripping equipment for 5 hours. The oily fraction was separated from the aqueous solution, obtaining 10.2 mL of essential oil, which was then dried with anhydrous sodium sulfate and stored under refrigeration using amber bottles. The obtained dried essential oil was then subjected to gas chromatography followed by mass spectroscopy analysis (GC-MS).

GC-MS analysis of the *Eucalyptus globulus* oil

Gas chromatography coupled to mass spectroscopy (GC-MS) analyses were performed using a Shimadzu QCMSQP2020 instrument, with a 30 m long Rxi ®-5Sil MS RETEK (Centre County, PA, U.S.) capillary column. The injection volume was 1 µL, a total flow rate of 21.6 mL/min, and the column flow rate of 0.60 mL/min; the temperature was programmed to be maintained at 60 °C for 1 min, then increased at a rate of 10 °C/min to be finally maintained for 6 min at 280 °C.

Validation of the Docking Protocol

The docking protocol was validated by Molecular Docking Using Chimera (University of California) and AutoDock Vina Software. A threshold value of 2.0 Å for Root Mean Square Deviation (RMSD) is generally accepted as the upper limit for validating a successful molecular docking pose against a reference structure. Interactions of the crystallographic structures, PDB ID: 6W63 (X77), PDB ID: 2GX4 (NOL), and PDB ID: 5RTY (HBD) were used for the validation of the protocol. The docking results showed similarity between the ligand pose and coordinated pose [RMSD = 0.22 Å (6W63), 0.49 Å (5RTY), and 0.71 Å (2GX4)], with a binding affinity of -3.25 kcal/mol (6W63), -3.777 kcal/mol (5RTY), and -4.181 kcal/mol (2GX4), respectively. These results demonstrated that the docking protocol used in this study was reliable, as the RMSD values were lower than the 2.0 Å upper limit.

1,8-cineole modeling

The structure of 1,8-cineole was modelled using density functional theory (DFT) with the B3LYP/6-31G basis set *in vacuo* (Spartan 18 software). The optimised molecule ($C_{10}H_{18}O$; molecular weight 154.25 amu) exhibited an energy of −467.14 a.u. and a dipole moment of 1.30 D. Frontier orbital energies were calculated as EHOMO = −6.24 eV and ELUMO = 1.86 eV. Predicted QSAR descriptors included molecular surface area (195.66 Å²), polar surface area (6.506 Å²), molecular volume (181.95 Å³), ovality (1.26), logP (1.86), and polarizability (54.22). The molecule has no hydrogen-bond donors and one hydrogen-bond acceptor.

Receptors for Docking with 1,8-cineole

Thirteen crystallographic structures of SARS-CoV-2 were selected as receptor structures for docking studies with 1,8-cineole (eucalyptol), the major component of *Eucalyptus* essential oil. The receptors included the SARS-CoV-2 main protease (M^{pro}/3CL/$3CL^{pro}$) and NSP3 macrodomain proteins (Table 1). All structures were retrieved from the RCSB PDB and prepared in UCSF Chimera before docking with AutoDock Vina.

The receptors were chosen based on the availability of high-resolution crystallographic data and the presence of co-crystallised inhibitors, which facilitated validation of the docking protocol. Binding efficacy was assessed using two main criteria: (i) the lowest value of binding energy (BE) referring to the most stable interaction and (ii) interactions with key active site residues, mainly hydrophobic interactions, since the ligand has no hydrogen-bond donors and only one hydrogen-bond acceptor. The amino acid sequences of the structures were also analyzed by multiple alignment using the Clustal Omega (1.2.4) server (www.ebi.ac.uk/Tools/msa/clustalo/).

Table 1. Molecular structures used to prepare the receptors.

Receptor	PDB code	Comments	Resolution (Å)
Main protease (M^{pro})	6LU7	In complex with an inhibitor N3	2.16
Main protease (M^{pro})	6W63	In complex with an inhibitor X77	2.10
Main protease (M^{pro})	6W79	In complex with an inhibitor X77	1.47
Main protease (M^{pro})	6XHL	In a covalent complex with the inhibitor	1.47
Main protease (M^{pro})	5REG	in complex with Z1545313172	1.67
Main protease (M^{pro})	5R81	in complex with Z1367324110	1.95
Main protease (M^{pro})	2A5K	In complex with an inhibitor, aza-peptide epoxide	2.30
Main protease (M^{pro})	2GX4	In complex with an inhibitor	1.93
Main protease (M^{pro})	2QIQ	Structure-based peptidomimetic inhibitor	1.90
NSP3 macrodomain (MacI)	5RSZ	in complex with ZINC000004218283	1.02
NSP3 macrodomain (MacI)	5RVC	in complex with ZINC000933940912	1.00
NSP3 macrodomain (MacI)	5RVR	in complex with ZINC000016052862	1.04
NSP3 macrodomain (MacI)	5RTY	in complex with ZINC000000157088	1.00

RESULTS

In Bolivia, the traditional use of eucalyptus leaves has been practiced for centuries, and it has been incorporated into various traditional medicinal systems. During the COVID-19 pandemic, in the Andean region of Bolivia, vaporized eucalyptus oil was used in many homes, including hospitals. Eucalyptus oil[30,31] was obtained by steam distillation of leaves collected in the town of Quime, La Paz, Bolivia. GC-MS analysis of eucalyptus oil revealed the presence of 1,8-cineole (eucalyptol), ca. 80 %, being the most abundant and the only oxygenated component in the mixture. In addition, 3-carene (12.3 %), o-cymene (2.6 %), and 2-bornylene (2.1 %) were also found in smaller proportions (Fig. 1). Considering the many previous reports on the pharmacological effects of 1,8-cineole, this work establishes an initial *in silico* study of this compound used in traditional medicine.

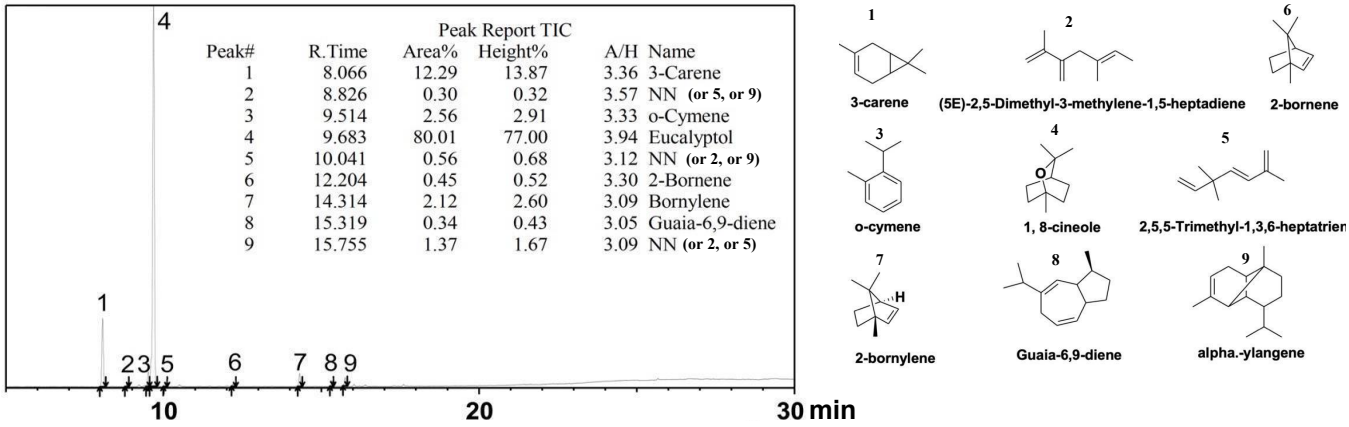

Fig. 1. Most abundant compounds in *Eucalyptus globulus oil*. GC-MS chromatogram

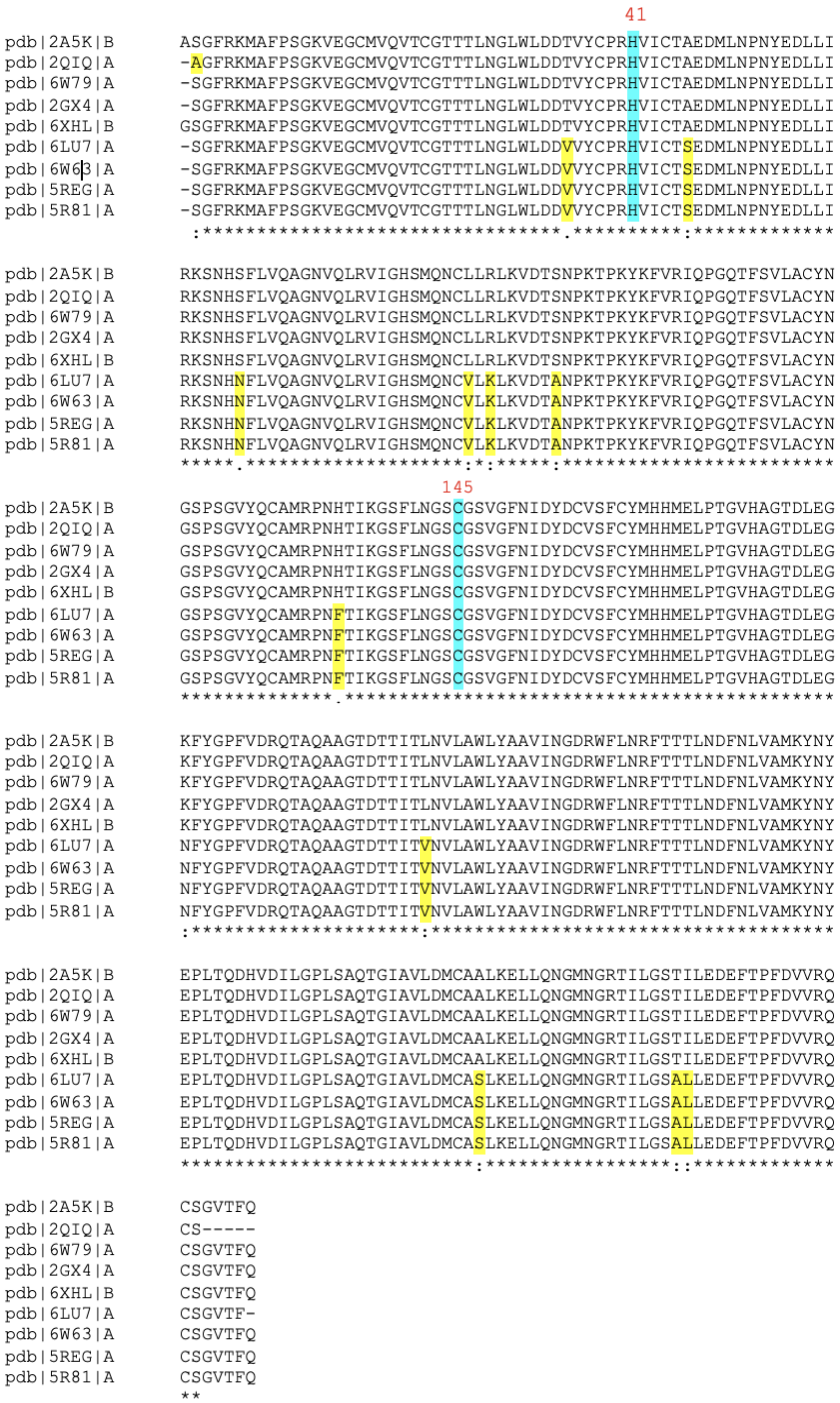

Amino acid sequence analysis

The multiple sequence alignment of amino acids showed identical sequences for the macrodomain (Mac1), whereas the main protease (M^{pro}) contained 11 mutations (Fig. 2). These mutations may be attributed to different viral strains. However, most of them are located far from the active site and are therefore unlikely to affect substrate binding or inhibitor interactions directly (Fig. 3). Only the Ser-46-Ala substitution lies at the entrance of the active site pocket in M^{pro} and could influence ligand interactions, since alanine is more hydrophobic and sterically smaller than serine. Future functional studies on this mutation would be of particular interest.

The hydrophobicity surface analysis showed that both M^{pro} and Mac1 have hydrophobic regions in their active sites (Fig. 3), which can facilitate interactions with hydrophobic ligands such as 1,8-cineole. In addition, Mac1 shows a significantly larger hydrophobic surface in its active site than M^{pro}, suggesting that it may represent a better target for 1,8-cineole. No other pockets were identified on the protein surface for potential ligand interactions, indicating that inhibitors are likely to bind within the active site pocket.

Figure 2. Multiple alignment of the main protease M^{pro} structures used as a receptor. In yellow, the mutations and in cyan, the catalytic amino acids. Where (*) denotes conserved or identical amino acid, (:) conservative or amino acid with similar biochemical property, (.) semiconservative.

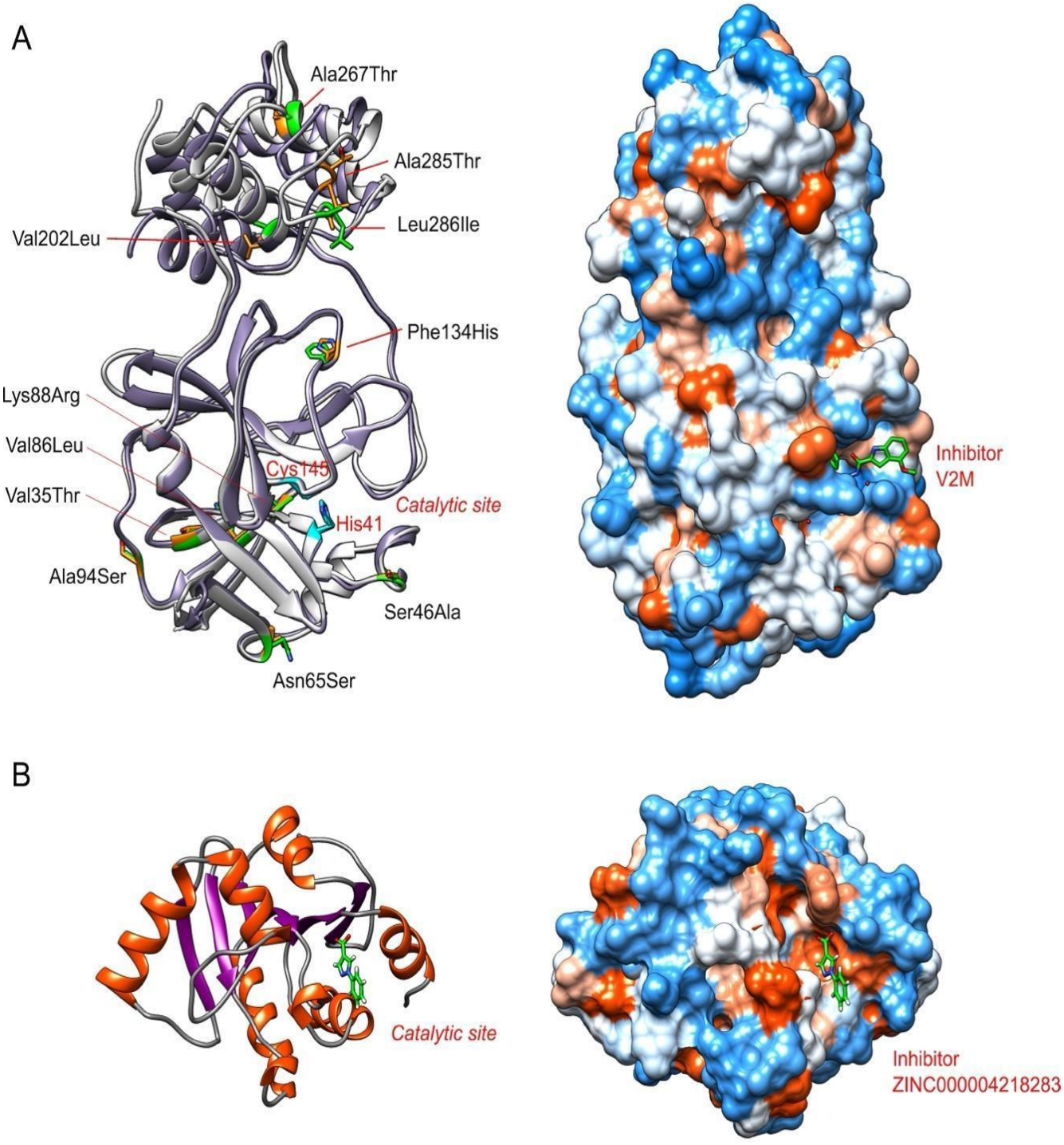

Figure 3. Molecular structures of the M^{pro} and Mac1 proteins. (A) Left: Overlapped M^{pro} proteins showing mutations (PDB: 6LU7 and 6XHL). Right: M^{pro} hydrophobicity surface and inhibitor V2M (PDB: 6XHL). (B) Mac1 protein with a ligand, ribbons, and hydrophobicity representations. The hydrophobic surfaces represent the non-polar residues in red and the polar ones in blue, and white represents areas of intermediate polarity.

Molecular docking between 1,8-cineole and M^{pro}

Molecular docking of 1,8-cineole with protein receptors (PDB ID): 6LU7, 6W63, 2GX4, and 5RTY revealed different poses of the ligand for each receptor (Table 2). The interatomic distances in the molecular interactions were lower than 6 Å in all cases. Results show hydrophobic interactions with Phe-140, Asn-142, Ser-144, Cys-145, His-163, and His-172 residues, while interaction with Glu-166, belonging to the S1 lateral chain of 6LU7, was also previously reported by Shana V. Stoddard et al [20].

Table 2. Summary of the most stable docking poses of 1,8-cineole with SARS-CoV-2 proteins M^{pro} and MacI.

Receptor	PDB	Best binding (kcal/mol)	Energy	Key interacting residues
Main protease (Mpro)	5R81	-5.402		His-163, Met-165, Glu-166, Cys-145, Asn-142.
	6W79	-4.944		Met-49, Cys-44, Phe-66, Asn-142.
	6XHL	-4.299		Met-165, Cys-145, Phe-140, Asn-142.
	6LU7	-4.287		Asn-142, Cys-145, Ser-144, Phe-140, Leu-141.
	2GX4	-4.181		Thr-25, Leu-27, His-41, Cys-44, Met-49, Asn-142.
	2A5K	-3.86		Met-165, Val-171, His-172, Thr-190.
	6W63	-3.25		Met-49, Asn-142, Glu-166, Gln-189.
	2QIQ	-3.149		Thr-25, His-41, Val-42, Met-49.
	5REG	-2.188		Pro-108, Ala-129, Val-202, Leu-242.
NSP3 Macrodomain (MacI)	5RVR	-6.380		Pro-125, Ala-129, Leu-160, Val-155.
	5RVC	-5.587		Pro-125, Ala-129, Leu-160, Val-155.
	5RSZ	-4.981		Pro-32, Ala-89, Val-121, Leu-123.
	5RTY	-3.777		Pro-125, Ala-129, Leu-160, Pro-136, Ile-131.

The most stable interaction between 1,8-cineole and M^{pro} was with 5R81, with an energy binding of -5.402, involving the following key residues: Glu-166, Met-165, Asn-142, His-163 and Cys-145 (Table 3 and Fig. 4). Comparing the complex 5R81/1,8-cineole with re-docked crystallographic complex 5R81/ ZINC_108126011, the last shows higher binding stability, ranging from -6.82 kcal/mol to -9.39 kcal/mol, in the most stable ligand pose. In this complex, the ligand ZINC_108126011 forms both hydrogen bonds and hydrophobic interactions with residues Met-165 and Glu-166 [21]. The most stable interaction can be attributed to the multiple hydrogen bonds formed by ZINC_108126011 with the receptor, while 1,8-cineole has only one hydrogen bond acceptor and lacks hydrogen-bond donor groups.

Table 3. Distance (Å) of molecular docking between 1,8-cineole and 5R81.

(kcal/mol)	His-163	Met-165	Glu-166	Cys-145	Asn-142
-5.402	2.546	3.874	3.251	3.308	3.516
-4.738	4.489	3.156	3.163	5.075	4.320
-4.620	4.335	3.201	3.296	4.969	5.143
-4.560	3.209	2.932	3.009	3.760	3.828
-4.554	2.750	2.985	4.435	4.064	3.732

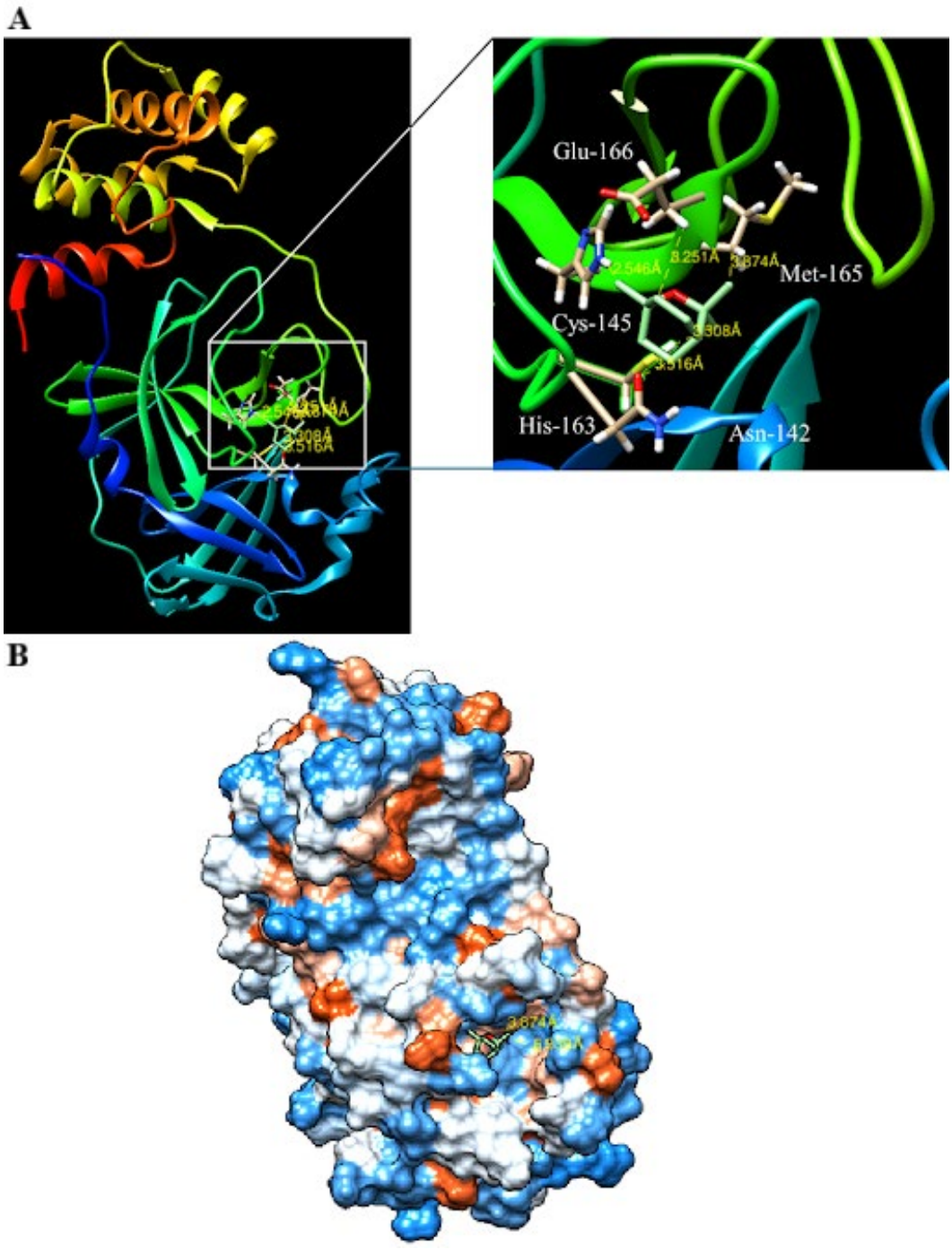

Figure 4. Complex M ^{pro} (5R81)/1,8-cineole. (A) Interactions of 1,8-cineole with Glu-166, Met-165, Asn-142, His-163 and Cys-145 of 5R81 (-5.402 kcal/mol). (B) Hydrophobicity representations of the receptor, the non-polar residues in red and the polar ones in blue, and white represents areas of intermediate polarity. The ligand is shown in sticks, green (C-atoms) and red (O-atom).

Molecular coupling carried out for 6W79 (-4.944 kcal/mol) revealed interactions with Met-49, Cys-44, Phe-66, and Asn-142, while docking for 6XHL (-4.299 kcal/mol) showed interactions with Met-165, Cys-145, Phe-140, and Asn-142, this latter one being a common residue between these two docking results in the present work. Binding energies (kcal/mol) between 1,8-cineole and 6LU7 were -4.287, -3.692, -4.229, -4.086, and -4.01, having interactions with

residues Gln-189, Asn-142, Ser-144, and His-163. Yet another study with 6UL7 revealed binding energy of –5.86 kcal/mol and 11 hydrophobic bonds with Met-49, Met-165, His-164, Arg-188, and Pro-52 amino acids; one pi-sigma interaction with His-41; and four van der Waals forces with Asp-187, Gln-189, Tyr-54, and Phe-181 residues [22]. Other studies with 6LU7 structure and essential oils from *Matricaria recutita* L. and *Zingiber ocinale* Roscoe showed sesquiterpene hydrocarbons (E, E)-farnesene and (E)-farnesene as the best scored ones, occupying the substrate binding site, flanked by Gln-189, Arg-188, Met-165, His-41, and Asp-187 [23]; all of them different from the ones found interacting with 1,8-cineol in this work. Binding energies (kcal/mol) of 1,8-cineole with 2GX4 were -4.181 (Table 2), -4.174, -4.13, -4.004, and -3.146, showing interactions with Thr-25 and His-41 residues that were of a hydrophilic nature, while interactions with Val-42 and Met-49 were of a hydrophobic nature. Binding energies (kcal/mol) of 1,8-cineole with 6W63 were -3.25 (Table 2) and -2.863, showing interactions with S1 at site residues Asn-142, Glu-166, Gln-189, and Met-49. Molecular docking of M^{pro} carried out with ligand X77 (PDB: 6W63) crystal structure revealed binding energy of -5.38 kcal/mol, where Gln-189 form a hydrogen-bond interaction, while, Met-49, Cys-44, His-41, Met-165, Arg-188, Pro-52, and Tyr-54 are involved in hydrophobic interactions [24], being the interacting residues Gln-189 and Met-49 common with the ones found in this work.

Molecular docking was also carried out for 2QIQ (-3.149), finding hydrophobic interactions interestingly with Thr-25, His-41, Val-42 and Met-49, the same residues described for 2GX4 (see above), while docking for 2A5K (-3.86) revealed hydrophobic interaction with Thr-190, His-172, Val-171 and Met-165; although similar residues, they were found in different positions. Molecular docking carried out for 5REG showed the least stable binding energy (-2.188 kcal/mol), finding Pro-108, Ala-129, Leu-242, and Val-202 as the hydrophobic interacting residues.

The interactions of 1,8-cineole with the target, M^{pro}, showed its capability of acting as an inhibitor, having had access to the hydrophobic region adjacent to Met-49 in the subsite S2 with 6LU7, 6W63, and 2GX4 (Table 2). There would also be a higher binding affinity in the Gln-189 residue in the main chain observed in 6LU7 and 6W63. Similarly, the hydrogen bonds formed by Ser-144, His-163, and Asn-142 observed with 6LU7 and 6W63, respectively, could confer high affinity.

Molecular docking between 1,8-cineole and MacI

The most stable interacting structure was found to be 5RVR with a binding energy of -6.380 kcal/mol and key interacting residues: Pro-125, Ala-129, Leu-160, and Val-155 (Table 4 and Fig. 5). Another pose of the ligand interacted with the same residues with a lower binding energy (-5.587 kcal/mol). Other binding energies (kcal/mol) of 1,8-cineole with 5RTY were -3.777, -3.66, -0.922, and -1.45; while the interacting residues were found to be Leu-160, Phe-156, Ala-129, Pro-136 and Ile-131. Except for Ala-129 and Pro-136, all of the hydrophobic residues occurred in flanking regions; hydrophobic propensity values for these residues are considered to be region *1* [25], enhancing in this way the access of 1,8-cineole to this hydrophobic zone, although Ala-129 is considered partially hydrophobic. Docking for 5RSZ (-4.981) showed hydrophobic interactions formed by Pro-32, Ala-89, Leu-123, and Val-121, the same four interacting residues involved in hydrophobic interactions in 5R81 and 5REG, although all of them in different positions (see above).

Table 4. Distance (Å) of molecular docking between 1,8-cineole and 5RVR.

(kcal/mol)	Leu-160	Val-155	Ala-129	Pro-125
-6.380	2.816	2.624	3.059	2.923
-6.151	2.741	2.935	3.133	2.753
-5.904	2.545	2.722	3.140	3.534
-5.878	2.768	2.750	3.537	4.823
-5.822	2.869	2.789	3.385	3.235
-5.719	3.023	2.642	2.892	3.549
-5.673	3.873	3.148	2.514	3.550
-5.520	2.700	2.665	2.880	3.338
-5,425	3.445	2.684	2.887	3.118
-5.369	3.361	3.665	3.077	4.402

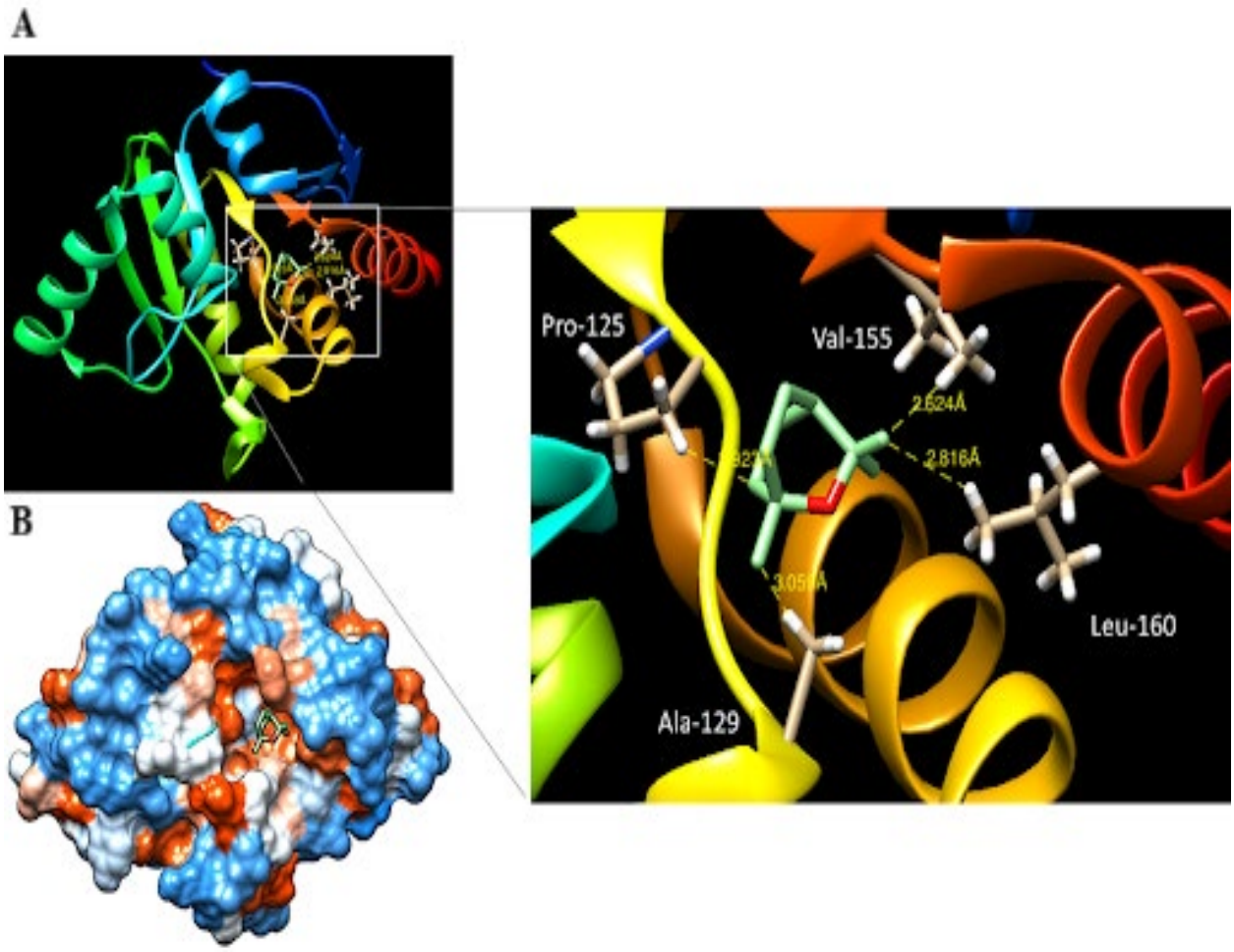

Figure 5. Complex MacI (5RVR)/1,8-cineole. (A) Interactions of 1,8-cineole with Pro-125, Ala-129, Leu-160, and Val-155 of 5RVR (-6.380 kcal/mol). (B) Hydrophobicity representations of the receptor, the non-polar residues in red and the polar ones in blue, and white represents areas of intermediate polarity. The ligand is shown in sticks, green (C-atoms) and red (O-atom).

DISCUSSION

Eucalyptus globulus leaves vapor was shown to be very active against the influenza virus following exposure for only 10 min [26]. Eucalyptus is widely used in traditional Bolivian medicine, particularly in the Andean and sub-Andean regions, primarily against colds in the winter. In the form of vapors in decoctions, as an antiseptic wound wash, in inhalations for bronchitis and catarrh, and in fumigations as an antiseptic and disinfectant.

Results of the work carried out by Shana V. Stoddard [20] indicate that the ensemble molecular docking study revealed several tools that can be utilized to optimize current drug candidates for SARS-CoV-2 M^{pro} and subsite binding preferences. Binding in the S1′, S2, and S4 subsites can all be facilitated by both hydrophobic interactions and hydrogen bonding interactions. The S2 subsite was one of the most prominent binding sites utilized in the inhibitor mode of binding to access the S2 subsite: the inclusion of hydrophobic substituents that can interact with Met-49, or the inclusion of hydrogen bonding donor or acceptors atoms, which can access the hydrogen bonding hotspot formed by the backbone of residues Asp-187, Arg-188, Gln-189, and the side chain of Tyr-54. Compounds can be developed to access the S1 subsite with high affinity by accessing the hydrogen bonding hotspot formed by Leu-141, Ser-144, His-163, and Asn-142.

Catalytic residues Cys-145 and His-41 found in interactions of 1,8-cineol with 2GX4 (Table 2), buried in an active site cavity located on the surface of the protein, were found to accommodate four substrate residues in positions P1’

through P4, flanked by residues from both domains I and II [13]. These amino acids were also found to have molecular interactions with five natural compounds, Withanosides V and VI, Racemosides A and B, and Shatavarin IX inhibitor candidates in previous molecular docking studies [27]. While in the present work, molecular docking allowed us to confirm ligand-receptor interactions based on binding energies between 1,8-cineole and crystal structures PDB: 6LU7, 6W63, 6W79, 6XHL, 5REG, 5R81, 5RSZ, 5RVC, 5RVR, 5RTY, 2GX4, 2QIQ, and 2A5K, relevant surface interactions were found to be only with 6LU7, 6W63, 2GX4, and 5RTY. Room-temperature structure of the ligand-free M^{pro} form may be the most physiologically relevant structure for performing molecular docking studies to estimate drug binding and enable drug design [13], thus validating the traditional use of oil vapor in the Andean region of Bolivia to prevent respiratory diseases.

The use of other docking software resources like 1-click Docking, PatchDock, and Swiss Dock software revealed interaction between 1,8-cineole and M^{pro} (-6.04 kcal/mol) in the binding pocket of the active site, which was mediated by two hydrophobic interactions through Met-6, Phe-8, Asp-295, and Arg-298 with no H-bond interactions [28]. The relatively weak binding for 1,8-cineole is consistent with its structural properties. It is a bicyclic terpenoid of low molecular weight, which results in a rigid structure that reduces its conformational adaptability, limiting its optimal binding with receptors. This small molecule is highly hydrophobic, interacting with the receptors almost exclusively through van der Waals and hydrophobic contacts. Based on these results, the use of 1,8-cineole may represent a possible treatment for COVID-19, acting as an inhibitor of M^{pro} [29]. It is of utmost importance to proceed with *in vitro* and *in vivo* studies since molecular docking lacks strong evidence; it only represents ligand-protein interaction and not the effect of the interaction, stabilizing or inhibiting.

CONCLUSIONS

This study investigated the molecular docking of 1,8-cineole with SARS-CoV-2 Mpro and the NSP3 macrodomain (MacI). The results showed modest but consistent binding energies between the 1,8-cineole and mainly hydrophobic residues in the active sites of both proteins. MacI presented larger hydrophobic cavities and stronger predicted affinities than Mpro, suggesting it may be a more favourable target for 1,8-cineole. These in silico results should be viewed as a preliminary step towards wet experiments. Experimental studies, including biochemical inhibition assays and antiviral tests, are required to validate whether 1,8-cineole or related derivatives have measurable activity against SARS-CoV-2. Given the traditional use of eucalyptus oil vapour in the Andean region for respiratory ailments, this study provides a first computational rationale for its potential relevance in antiviral research.

ACKNOWLEDGEMENT

To Mr. Santiago Tarqui, research technician from Chemical Research Institute IIQ-UMSA, for realization of GC-MS analysis.

REFERENCES

[1] Z. M. Cai, J. Q. Peng, Y. Chen, L. Tao, Y. Y. Zhang, L. Y. Fu, Q. D. Long, X. C. Shen, *J Asian Nat Prod Res*, 2021, **23**, 938. https://doi.org/10.1080/10286020.2020.1839432

[2] C. H. Cosima, J. Petry, L. Griesbaum, T. Weiser, K. Werner, M. Ploch, A. Verschoor, G. Multhoff, A. B. Dezfouli, B. Wollenberg, *Biomedicine & Pharmacotherapy*, 2023, **167**, 115467. https://doi.org/10.1016/j.biopha.2023.115467 .

[3] Y. Cui, Q. Zhang, K. Yin, N. Song, B. Wang, H. Lin, *Ecotoxicology and Environmental Safety*, 2020, 206, 111151, https://doi.org/10.1016/j.ecoenv.2020.111151

[4] A. A. Akhmouch, S. Hriouech, A. Mzabi, M. Tanghort, H. Chefchaou, A. Remmal, N. Chami, *Antibiotics*, 2022, **11**, 1002. https://doi.org/10.3390/antibiotics11081002

[5] J. S. Kumar, S. Umesha, K. S. Prasad, P. Niranjana, *Curr Microbiol.*, 2016, **72**, 297. DOI: 10.1007/s00284-015-0953-0.

[6] S. Z. A. Molaeitabari, T. Sultana, T. E. S. Dahms, *Microorganisms*, 2022, **10**, 1989. DOI: 10.3390/microorganisms10101989

[7] L. Qu, T. Chai, Z. Guo, Z. Zhang, Z. Huang, N. Li, *Poultry Science*, 2024, **103**,103365. https://doi.org/10.1016/j.psj.2023.103365

[8] A. Al-Ahmad, P. Zou, D. L. Solarte, E. Hellwig, T. Steinberg, K. Lienkamp, *PLoS One*, 2014, **9**, e111357. DOI: 10.1371/journal.pone.0111357

[9] C. S. Cox, *Science Progress*, 1989, **73**, 469. https://www.jstor.org/stable/43421049

[10] D. Verreault, S. Moineau, C. Duchaine, *Microbiol Mol Biol Rev.*, 2008, **72**, 413. DOI: 10.1128/MMBR.00002-08

[11] T. Pillaiyar, M. Manickam, V. Namasivayam, Y. Hayashi, S. H. Jung, *J Med Chem.* 2016, **59**, 6595. DOI: 10.1021/acs.jmedchem.5b01461
[12] Z. Jin, X. Du, Xu, Y. et al., *Nature*, 2020, **582**, 289. https://doi.org/10.1038/s41586-020-2223-y .
[13] D. W. Kneller, , G. Phillips, , H. M. O'Neill, et al. *Nat Commun,* 2020, **11**, 3202. https://doi.org/10.1038/s41467-020-16954-7
[14] T. Ertan-bolelli , K. Bolelli , C. Altunayar-unsalan , O. Ünsalan , B. Yılmaz Ertan-bolelli, *Turkish Computational and Theorical Chemistry*, 2023, **7**. https://doi.org/10.33435/tcandtc.1151841
[15] M. S. Fernandes, F. S. da Silva, A. C. S. G. Freitas, E. B. de Melo, G. H. G. Trossini, F. R. Paula, *Molecular Informatics*. 2021, **40**, e2000096, https://doi.org/10.1002/minf.202000096
[16] E. Yuanita, S. Sudirman, N. K. T. Dharmayani, M. Ulfa, S. Hadisaputra, J. Syahri, *Molekul*, 2022, **17**, 1. https://doi.org/10.20884/1.jm.2022.17.1.5600
[17] https://arxiv.org/abs/2102.13468. Access date: September 2025
[18] M. Iqhrammullah, D. R. Rizki, A. Purnama, T. F. Duta, H. Harapan, R. Idroes, B. Ginting, *Scientia Pharmaceutica*, 2023, **91**, 15. https://doi.org/10.3390/scipharm91010015
[19] P. González-Maldonado, N. Alvarenga, A. Burgos-Edwards, M. E. Flores-Giubi, J. E. Barúa, M. C. Romero-Rodríguez, R. Soto-Rifo, F. Valiente-Echeverría, P. Langjahr, G. Cantero-González, P. H. Sotelo, *Molecules*, 2022, **27**, 1743. https://doi.org/10.3390/molecules27051743
[20] Shana V. Stoddard, Et. al., *Viruses*, 2020, **12**, 942. https://doi.org/10.3390/v12090942
[21] N. Razzaghi-Asl, A. Ebadi, S Shahabipour, D. Gholamin, *J Biomol Struct Dyn.*, 2021, **39**, 6633. https://doi.org/10.1080/07391102.2020.1797536
[22] S. Panikar, G. Shoba, M. Arun, J. J. Sahayarayan, A. Usha Raja Nanthini, A. Chinnathambi, S. A. Alharbi, O. Nasif, H. J. Kim, *J Infect Public Health*, 2021, **14**, 601. DOI: 10.1016/j.jiph.2020.12.037
[23] J. K. R. D. Silva, P. L. B. Figueiredo, K. G. Byler, W. N. Setzer, *Int J Mol Sci.* 2020, **21**, 3426. https://doi.org/10.3390/ijms21103426
[24] I. N. Fitriani, W. Utami, A. T. Zikri, P. Santoso, *Research Square*; 2020, PREPRINT (Version 1) available at Research Square: https://doi.org/10.21203/rs.3.rs-42747/v1
[25] S. M. Gowder, J. Chatterjee, T. Chaudhuri, K. Paul, *The Scientific World Journal*, 2014, ID 971258. http://dx.doi.org/10.1155/2014/971258 .
[26] S. Vimalanathan, J. Hudson, *American Journal of Essential Oils and Natural Products*, 2014, **2**, 47-53. https://www.essencejournal.com/archives/2014/2/1/A/8
[27] C. N. Patel, S. P. Jani, D. G. Jaiswal, S. P. Kumar, N. Mangukia, R. M. Parmar, R. M. Rawal, H. A. Pandya, *Sci Rep.* 2021, **11**, 20295. https://doi.org/10.1038/s41598-021-99165-4
[28] A. D. Sharma, I. Kaur, *Notulae Scientia Biologicae*, 2020, **12**, 536–545. https://doi.org/10.15835/nsb12210711
[29] D. Mieres-Castro, S. Ahmar, R. Shabbir, F. Mora-Poblete. *Pharmaceuticals (Basel)*, 2021, **14**, 1210. DOI: 10.3390/ph14121210
[30] N. Čmiková, L. Galovičová, M. Schwarzová, M. D. Vukic, N. L.Vukovic, P. Ł. Kowalczewski, L. Bakay, M. I. Kluz, C. Puchalski, M. Kačániová, *Plants*, 2023, **12**, 1076. https://doi.org/10.3390/plants12051076
[31] https://copilot.microsoft.com/shares/ns87Hbzc7gR1MBp5BzfGN. Access date: September 2025